This is the initially submitted version of the paper "M. Cardoso Dos Santos, J. Goetz, H. Bartenlian, K.-L. Wong, L.J. Charbonnière, and N. Hildebrandt. Autofluorescence-free Live-cell Imaging Using Terbium Nanoparticles. *Bioconjugate Chemistry* **2018**, 29, 1327–1334." DOI: 10.1021/acs.bioconjchem.8b00069; https://pubs.acs.org/doi/10.1021/acs.bioconjchem.8b00069.

Autofluorescence-free Live-cell Imaging Using Terbium Nanoparticles

M. Cardoso Dos Santos,[1] J. Goetz,[2] H. Bartenlian,[1] K.-L. Wong,[3] L.J. Charbonnière,[2*] N. Hildebrandt[1*]

[1] NanoBioPhotonics (nanofret.com), Institute for Integrative Biology of the Cell (I2BC), Université Paris-Saclay, Univeristé Paris-Sud, CNRS, CEA, 91405 Orsay Cedex, France

[2] Laboratoire d'Ingénierie Moléculaire Appliquée à l'Analyse (LIMAA), Institut Pluridisciplinaire Hubert Curien (IPHC), CNRS, Université de Strasbourg, 67087 Strasbourg Cedex, France

[3] Department of Chemistry, Hong Kong Baptist University, Hong Kong SAR, Hong Kong

ABSTRACT: Fluorescent nano-particles (NPs) have become irreplaceable tools for advanced cellular and sub-cellular imaging. While very bright NPs require excitation with UV or visible light, which can create strong autofluorescence of biological components, NIR-excitable NPs without autofluorescence issues exhibit much lower brightness. Here, we show the application of a new type of surface-photosensitized terbium NPs (Tb-NPs) for autofluorescence-free intracellular imaging in live HeLa cells. Combination of exceptionally high brightness, high photostability, and long photoluminecence (PL) lifetimes for highly efficient suppression of the short-lived autofluorescence, allowed for time-gated PL imaging of intracellular vesicles over 72 h without toxicity and at extremely low Tb-NP concentrations down to 12 pM. Detection of highly resolved long-lifetime (ms) PL decay curves from small (~10 μm^2) areas within single cells within a few seconds emphasized the unprecedented photophysical properties of Tb-NPs for live-cell imaging that extend well beyond currently available nanometric imaging agents.

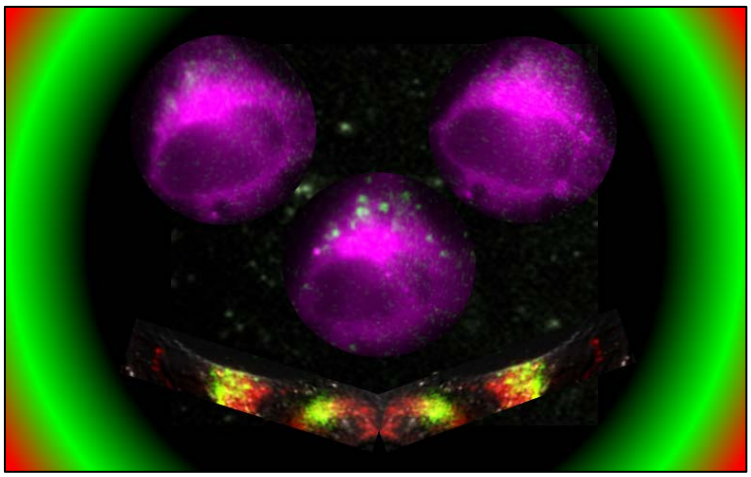

KEYWORDS: *Lanthanides, Time-gating, Microscopy, Nanocrystals, Endocytosis*

This is the initially submitted version of the paper "M. Cardoso Dos Santos, J. Goetz, H. Bartenlian, K.-L. Wong, L.J. Charbonnière, and N. Hildebrandt. Autofluorescence-free Live-cell Imaging Using Terbium Nanoparticles. *Bioconjugate Chemistry* **2018**, 29, 1327–1334." DOI: 10.1021/acs.bioconjchem.8b00069; https://pubs.acs.org/doi/10.1021/acs.bioconjchem.8b00069.

Over the last two decades, fluorescence bioimaging has witnessed tremendous advances by the application of nanoparticles (NPs), such as quantum dots,[1,2] carbon dots,[3,4] polymer NPs,[5-7] nanodiamonds,[8,9] upconversion NPs,[10-12] or lanthanide NPs.[13,14] While all of these NPs comprise specific and unique photophysical and photochemical advantages for different imaging applications, one usually has to make a choice between high brightness (quantum dots, polymer NPs, nanodiamonds) or efficient autofluorescence background suppression (upconversion and lanthanide NPs). However, NPs that combine high brightness with autofluorescence-free detection for photostable and non-toxic imaging inside live cells down to the single-cell level at very low NP concentrations have yet to be demonstrated. Upconversion NPs can be excited in the NIR, which is a wavelength range that does not significantly excite endogenous biological components, and therefore strongly reduces autofluorescence. On the other hand, excitation of upconversion NPs is a very inefficient multi-photonic process that leads to very weak absorption cross sections and very low quantum yields.[12] Time-gated photoluminescence (TG-PL) detection of long-PL-lifetime (µs to ms) lanthanide fluorophores can efficiently suppress the shorter-lifetime autofluorescence (ns to µs) of biological samples by measuring PL intensities in detection windows that are temporally delayed by several µs after the excitation pulse.[15,16] To circumvent the very low absorption cross sections of lanthanide ions, their excitation is usually performed via sensitizers. TG-PL imaging has been successfully implemented using lanthanide complexes composed of an antenna ligand and a central lanthanide ion.[16-18] The main limitation for these molecular complexes is the low photon flux (number of photons per time) because, despite the relatively high brightness, pulsed excitation with low repetition rates (usually between 10 and 300 Hz, whereas conventional fluorescent dyes can be excited with repetition rates in the MHz range) is required for their long excitation-fluorescence cycles (PL lifetimes up to ms). One possibility to circumvent this problem is to increase the local concentration of lanthanide emitters inside NPs. Silica NPs doped with Tb-

complexes have been applied for DNA hybridization assays using time-gated spectroscopy.[19] Bright lanthanide-doped NPs, in which the emitting lanthanide ions were efficiently sensitized by transition-metal complexes[20] or the polymer matrix of the NPs,[21] were also developed for cellular imaging. However, their TG-PL imaging performance remained in a proof-of-concept stage.

In this work, we show that ultra-bright $La_{0.9}Tb_{0.1}F_3$ NPs with Tb-sensitizing antenna ligands on the NP surface can go far beyond confocal microscopy,[22] for which the steady-state UV excitation can lead to significant cell damage. Low repetition rates of short UV laser pulses led to extremely low excitation powers far below conventional microscopy setups and were therefore completely harmless for the cells and caused no photobleaching of the Tb-NPs. TG-PL detection allowed for autofluorescence-free imaging in live cells without the necessity of using specific non-fluorescent cell culture medium. Extremely low concentrations (down to 10 pM of Tb-NPs incubated with HeLa cells) were used for TG Tb-NP imaging and the cellular uptake by endocytosis could be followed over 72 h without any visible toxic effects on cell morphology. The very high brightness of the Tb-NPs was demonstrated by live-cell TG-PL imaging of single intracellular vesicles (late endosomes or lysosomes) that contained only few Tb-NPs and by the acquisition of entire Tb-NP PL decay curves (over 10 ms with 2.7 µs resolution) from a small (*ca.* 10 μm^2) area within a single cell, which were in excellent agreement with decay curves of Tb-NPs measured in solution.

RESULTS AND DISCUSSION

$La_{0.9}Tb_{0.1}F_3$ NPs were produced by microwave irradiation or a hydrothermal method in a heating oven and surface-functionalized with photosensitizing ligands as described in a previous study.[22] The Tb-NPs' high brightness (316,800 $M^{-1}cm^{-1}$; molar extinction coefficient multiplied by quantum yield) is mainly caused by their extremely large extinction coefficients of more than 5

mio. $M^{-1}cm^{-1}$, which largely compensate the moderate PL quantum yields (~3%). A detailed characterization (TEM, XRD, absorption and emission spectra, PL decays, quantum yields, and number of surface ligands) of the Tb-NPs used in the present study can be found in the Supporting Information. Most important for our live-cell imaging study was the very efficient excitation (via the antenna ligands on the NP surfaces) with a pulsed UV laser (349 nm, 100 Hz repetition rate, pulse duration ~15 ns, ~0.4 µJ on the sample), which resulted in very bright PL of the ligand-sensitized surface-near Tb^{3+}-ions inside the NPs with a main emission peak around 545 nm. For image acquisition, samples were excited with 400 pulses (gate number), which corresponded to a total exposure time of 6 µs (400 x 15 ns). Taking into account the illumination area of $5x10^{-4}$ cm^2, the irradiance was 80 mW/cm^2 (0.4 µJ x 100 Hz / $5x10^{-4}$ cm^2), and the light dose (irradiance multiplied by exposure time) was ~0.5 $\mu J/cm^2$. This irradiation dose is extremely low, even for UV irradiation. Research on photomutagenicity of cosmetic compounds showed a lack of phototoxicity of UVA light (365 nm) at a dose of 6.5 J/cm^2 ($13x10^6$-fold higher than our dose).[23] Investigations of antioxidants in green tea showed that UVA did not have significant impact on HaCaT cell survival at doses up to 5 J/cm^2 ($10x10^6$-fold higher than our dose).[24] In another study, UVA irradiation of cells with doses up to 7.5 J/cm^2 ($15x10^6$-fold higher than our dose) did not result in significant cytotoxicity and 2.5 - 7.5 J/cm^2 were considered as low UVA doses.[25] Imaging of live cells with repeated light exposure over 72 h experimentally confirmed the lack of phototoxic effects by using our low-dose pulsed UV irradiation concept (*vide infra*).

Tb-NPs with concentrations of 0.15 nM were sonicated and then incubated with HeLa cells in a standard culture medium (with serum and antibiotics) supplemented with HEPES buffer in order to prevent pH variations. Bright field images (DIC – differential interference contrast) and TG-PL images (with a delay time of 0.01 ms and gate time of 1.9 ms after the excitation pulse) of live HeLa cells were acquired in a live-cell chamber on an inverted wide-field microscope.

Throughout the present study, we used 400 excitation pulses at a repetition rate of 100 Hz for the acquisition of TG-PL images. Although the resulting acquisition time of 4 s allowed for an enhanced signal-to-noise ratio, 200 pulses and repetition rates of up to 300 Hz (2/3 s acquisition time) were found to provide images of sufficient quality (data not shown) in case faster processes need to be analyzed.

Tb-NPs were spontaneously uptaken by HeLa cells. To elucidate the uptake kinetics and intracellular fate of the Tb-NPs, we imaged live HeLa cells after 1, 3, 6, 24 and 72 h of incubation with 0.15 nM Tb-NPs (Figure 1). Because TG-PL microscopy is autofluorescence-free, we were not obliged to use a non-fluorescent medium (recommended for fluorescence microscopy) and cells were kept in the same culture medium without washing, during all incubation times. After 1 h of incubation, Tb-NPs had not yet penetrated into cells. Some Tb-NPs were perceptible outside the cells (red arrows in Figure 1), whereas others were attached to the plasma membrane (yellow arrows in Figure 1). Imaging after 3 h of incubation clearly revealed that a large part of Tb-NPs had entered inside the cells and vesicles carrying Tb-NPs were mainly organized around the cell nuclei (blue arrows in Figure 1). Longer incubation (up to 72 h) showed that Tb-NPs remained inside the cells without any visible change in cell morphology. Taking into account a cell cycle of approximately 20-24 h for HeLa cells,[26] we assume that Tb-NPs remain into daughter cells during cell division, a property that was also found for other NPs.[27] Most importantly, the Tb-NPs were not quenched by the cell environment and retained their initial brightness even after 72 h of incubation. Moreover, cell morphologies were perfectly preserved, which indicated that the spontaneous endocytosis of Tb-NPs did not significantly affect the live HeLa cells. In contrast, cell morphologies significantly changed, when the culture medium pH was not buffered by HEPES (Supporting Figure S6), which shows the general sensitivity of the cells to environmental changes and underlines the lack of toxicity of Tb-NPs. To further investigate possible toxic effects of our

Tb-NPs, we performed MTT cell viability test. Cells were incubated with Tb-NPs for 24h and the mitochondrial activity through reduction of the tetrazolium dye (MTT) to formazan was measured by absorption spectroscopy. Optical density values of formazan in control cells were 0.28, whereas those of cells incubated with Tb-NPs were 0.25 (for 0.12 nM Tb-NPs) and 0.24 (for 1.2 nM Tb-NPs), which corresponded to cell viabilities of 90 % and 84 % and confirmed an almost negligible cytotoxicity of Tb-NPs.

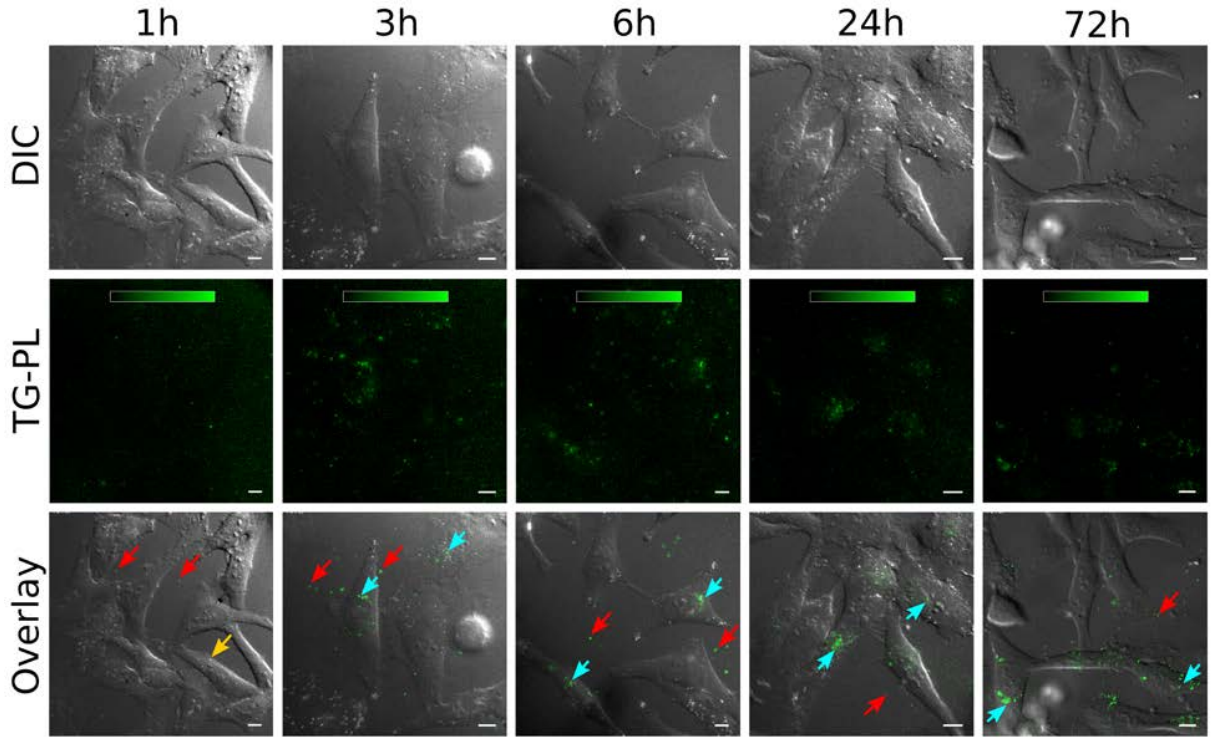

Figure 1. Live-cell images of 0.15 nM Tb-NPs incubated for different durations (given on top) with HeLa cells. Red arrows indicate Tb-NPs outside cells, yellow arrow Tb-NPs attached to the plasma membrane, and blue arrows Tb-NPs inside the cells. DIC: Differential interference contrast images; TG-PL: Time-gated photoluminescence images; Overlay: DIC overlaid with TG-PL. Color bars on TG-PL images: 1000-5000 counts. Scale bars: 10 µm.

To obtain more quantitative information about the uptake dynamics, we analyzed the number and intensity of intracellular vesicles (using the spot-detector function in Icy[28]) after 3, 6, 24, and 72 h of incubation (Table 1 and Supporting Figure S7). In order to efficiently study the

photophysical properties of the Tb-NPs, we selected those cells that provided the highest luminescence intensities. Although the spot area distribution was relatively broad (Supporting Figure S8), it did not vary significantly over time and showed a clear accumulation of spots with small diameters (average values between 0.24 and 0.28 μm^2), which were in excellent agreement with the diameter (~0.5 μm) of late endosomes in HeLa cells.[29,30] The different intensities of the spots indicate that the vesicles contained different amounts of Tb-NPs and although the detected vesicle area included ~5 pixels on the camera detector, the lateral resolution of our wide-field microscope did not allow for the distinction of single Tb-NPs. Another finding of the quantitative analysis was the average number of detected vesicles per cell, which slightly increased (~24 %) from 3 to 6 h of incubation and then dropped (~6 %) from 6 to 24 h and dropped even more (~24 %) from 24 to 72 h. This decrease was lower than expected (one would expect 50% of luminescent endosomes per cell after cell division) because we did not need to wash the cells after incubation (*vide supra*). Therefore, additional endocytosis of NPs that were still present in the cell medium was possible. The results confirm our earlier finding of an increasing uptake during the first 6 h of incubation and that cell division led to a distribution of the Tb-NPs in daughter cells. Further analysis of randomly selected cells (n = 16) at different times of incubation allowed us to observe the same tendency of NP uptake, which increased from 3 to 6h (16 %) and then progressively dropped (15 % from 6 to 24 h and 16 % from 24 to 72 h, data not shown). Although the distribution of NPs per cell was more heterogeneous for randomly selected cells (between 2 and 59 NPs, depending on the cell size) all cells analyzed from three different images contained Tb-NPs.

Table 1. Quantitative analysis of Tb-NP uptake in HeLa cells

Incubation time (h)	Cell number[a]	$\langle N_{spot} \rangle$[b]	$\langle A_{spot} \rangle$ (μm^2)[c]	$\langle I_{PL} \rangle$ (counts)[d]
3	7	25	0.24±0.24	2260±450
6	7	31	0.28±0.24	2280±560
24	6	29	0.25±0.26	2670±390
72	12	22	0.27±0.42	2360±550

[a] Number of cells analyzed on several TG-PL images. [b] Average spot number per cell. [c] Average spot area (± standard deviation). [d] Average PL intensity of all analyzed spots (± standard deviation). Note: Distribution diagrams (probability density of spot area) for the different incubation times are shown in Supporting Figure S8.

To confirm the localization of Tb-NPs in intracellular vesicles, as shown in a previous study using co-localization of Tb-NPs with a Lysotracker dye,[22] we performed different co-staining experiments and live-cell imaging after 24 h of incubation. The carbocyanine dye $DiOC_6(3)$ has a double hydrophilic-hydrophobic pattern, which allows it to insert and diffuse in phospholipid bilayers. Because of short carbon chains, the dye permeates across the plasma membrane and associates with intracellular lipid bilayers. At high concentrations (μM), $DiOC_6(3)$ intercalates endocytic compartments and membranes of the endoplasmic reticulum.[31] The overlay images in Figure 2A show three types of signals. Red areas indicate membranes of the endoplasmic reticulum (only $DiOC_6(3)$), green spots present Tb-NPs (attached to the microscope slide and plasma membranes or inside intracellular vesicles without $DiOC_6(3)$ staining), and yellow spots show a co-localization of Tb-NPs inside intracellular vesicles and $DiOC_6(3)$ in the membranes of these vesicles. To corroborate the intracellular location of the Tb-NPs we stained the plasma membrane with DiD and performed z-scan imaging through several live HeLa cells. The images in Figure 2B show a vertical scan (in steps of 1 μM) through two cells (an entire cell in the center and a part of another cell on the bottom right) and the Tb-NPs (green spots) light up within the cells (between z+3 μm and z+6 μm) whereas the green signal is rather faint above and below. The magenta

membrane staining helped to distinguish the cell contour from the intracellular localization of Tb-NPs. Taken together, the co-staining experiments clearly demonstrate that Tb-NPs are mainly located in endosomes/lysosomes.

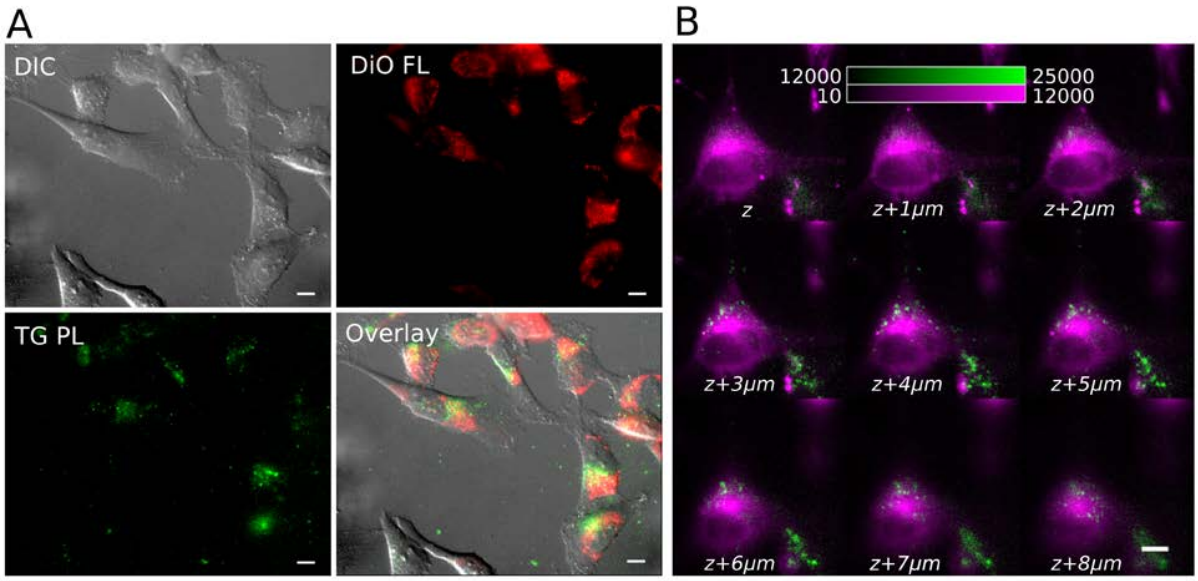

Figure 2. (A) Live-cell images of HeLa cells co-incubated for 24 h with $DiOC_6(3)$ and Tb-NPs$DiOC_6(3)$ fluorescence (DiO FL) is shown in red and was measured with steady-state detection whereas Tb-NP PL (TG PL) is shown in green and was measured with TG-PL. Yellow areas (in the overlay image) indicate co-localization of $DiOC_6(3)$ and Tb-NPs in intracellular vesicles.(B) 2D montage of different planes across HeLa cells co-incubated for 24 h with DiD (in magenta) and Tb-NPs (in green)Scale bars: 10 µm.

To further illustrate the exceptional brightness of Tb-NPs for intracellular TG-PL imaging, we incubated them at concentrations between 0.012 and 1.2 nM with HeLa cells for 24 h. At the highest incubation concentration (1.2 nM), which is already quite low compared to other NPs (for steady-state imaging of quantum dots we typically use a concentration of 5 nM in order to obtain sufficient signal), we could observe very bright Tb-NP PL, which was mainly situated inside cells and provided signal-to-noise ratios of up to 40 (Figure 3A middle row). Due to the absence of autofluorescence in the TG-PL mode, we could clearly visualize Tb-NPs at concentrations down to 0.012 nM with signal-to-noise ratios up to 5 (Figure 3A, bottom row). For all three different

concentrations, the Tb-NPs could be readily observed by looking through the microscope binocular, which was another indicator for their strong PL.

Encouraged by the outstanding brightness, we challenged the Tb-NPs with PL decay detection from a single cell. Phosphorescence lifetime imaging microscopy (PLIM) using luminescent metal complexes with microsecond PL lifetimes has become a frequently applied technique to exploit long PL lifetimes for the analysis of cells and tissues.[32] Millisecond PL lifetime imaging is much less frequent because of the necessary low excitation-pulse repetition rates (<1 kHz), which result in very long acquisition times of PL decay curves from conventional lanthanide complexes or NPs with limited brightness. Temporal sampling lifetime imaging microscopy (TSLIM) on confocal microscopes can circumvent these limitations and was successfully applied by using Eu and Tb complexes.[33,34] Our aim was the use of Tb-NPs for lifetime imaging on a conventional widefield microscope, which may become possible due to the unprecedented brightness of our millisecond emitters. We incubated 2 nM Tb-NPs for 24 h with HeLa cells and used a prototype lifetime imaging system (Horiba Jobin Yvon) for the selection of specific areas within cells for PL decay measurements. In this system, which was installed on a standard microscope output, the optical aperture of the light originating from the sample can be decreased by an adjustable mechanical diaphragm, such that only a part of the image can reach a PMT detector or a monocular, depending on which light path is selected by a mirror system. Visualization through the monocular allowed us to select a small area (*ca.* 10 μm^2) within a single cell, from which the PL was collected for detecting (in 4125 detection windows of 2.67 µs) a highly resolved PL decay curve over 10 ms within only 24 s. This intracellular Tb-NP decay was only slightly faster compared to the Tb-NP decay in solution (Figure 3B), which demonstrated the stability and preservation of photophysical properties of Tb-NPs in the cellular environment. A

control lifetime measurement on unstained cells (inset in Figure 3B) revealed a much shorter decay of the autofluorescence of the cell and cell culture medium, which underlined the advantage of TG-PL for efficient autofluorescence background suppression.

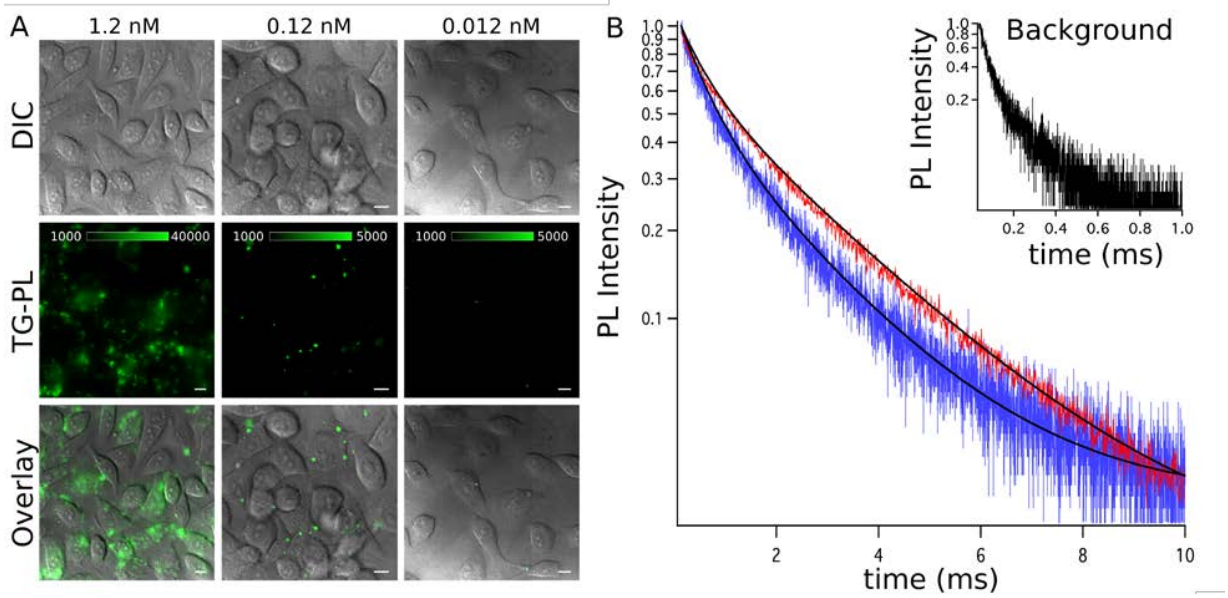

Figure 3. (A) Live-cell images of Tb-NPs incubated for 24 h at different concentrations (given on the top) with HeLa cells. (B) PL decays of Tb-NPs from a single HeLa cell (blue curve) and in solution (red curve). Mathematical fits shown in black. The inset represents PL emission from an unstained cell. Curves were intensity normalized at t=130 µs (t = 40 µs in the inset). Scale bars: 10µm.

CONCLUSION

We have demonstrated that ultra-bright Tb-NPs, in which the Tb-ions within the NPs are efficiently excited via photosensitizing ligands on the NP surface, can be highly advantageous for autofluorescence-free TG-PL imaging. The Tb-NPs were spontaneously endocytosed by HeLa cells within a few hours and retained their brightness over at least 72 h within intracellular vesicles without any visible cell damage. Single intracellular vesicles that contained only few Tb-NPs could be visualized and the autofluorescence-free TG-PL detection allowed for the use of extremely low concentrations (down to 12 pM) of Tb-NPs to be incubated with HeLa cells without the necessity to use non-fluorescent cell culture medium. The exceptional brightness of Tb-NPs was further

evidenced by the measurement of highly resolved long-lifetime (few ms) PL decay curves from small areas of single cells within only 24 seconds. The unique combination of high brightness, efficient autofluorescence background suppression, high and long-term photostability, and spontaneous cellular uptake for intracellular fluorescence imaging without toxic effects make these new Tb-NPs powerful tools for molecular fluorescence imaging beyond the currently available fluorescent nanomaterials.

MATERIALS AND METHODS

Terbium nanoparticles (Tb-NPs). Tb-NPs were prepared according to previously published procedures using 3,3'-((butane-1,4-diylbis(azanediyl))bis(carbonyl))bis(2-hydroxybenzoic acid) as a capping ligand (ligand L11).[22] NPs of batches 1 and 3 were obtained by the same protocol, whereas NPs for the second batch were obtained by a hydrothermal method (*vide infra*). TEM and XRD analyses of the as obtained NPs were collected (Figure S1 and S2) and compared to the previously published one, showing the same morphology and crystallographic properties than their microwave synthesized counterpart.[22] TEM measurements were carried out on a Tecnai G2 20 S-TWIN transmission electron microscope operating at an acceleration voltage of 200kV with a point-to-point resolution of 0.18 nm. Powder X-ray diffraction (XRD) patterns of the as-prepared NPs were recorded using Bruker AXS D8 Advance X-Ray Diffractometer at 40 kV and 40 mA with Cu-Ka radiation (Kα 1.5406 °A). The step scan covered the angular range from 15 to 75 in steps of 0.02. Photographs of the Tb-NPs at different steps of the preparation are shown in Figure S3.

Synthesis of Tb-NPs. Batches 1 and 3 were prepared in a microwave oven.[22] To a stirred aqueous mixture of $LaCl_3$ (14.4 mL, 0.05 M) and $TbCl_3$ (1.6 mL, 0.05 M) was added dropwise at room temperature a solution of NH_4F (3.51 mL, 0,72 M) in water, resulting in a cloudy solution. The

mixture was heated in a microwave oven at 150 °C for 12 min. After cooling, the precipitate was collected by centrifugation at 9000 rd/min for 25 min. The isolated solid was dispersed in 30 mL of milliQ water and sonicated at 60 °C for 1h. Batch 2 was prepared in a heating oven. To a stirred aqueous mixture of $LaCl_3$ (14.4 mL, 0.05 M) and $TbCl_3$ (1.6 mL, 0.05 M) was added dropwise at room temperature a solution of NH_4F (3.51 mL, 0,72 M) in water, resulting in a cloudy solution. The mixture was placed in a sealed tube and heated in a oven for 2 hours at 150 °C. After cooling, the precipitate was collected by centrifugation at 9000 rd/min for 25 min. The isolated solid was dispersed in 30 mL of milliQ water and sonicated at 60 °C for 1h.

Determination of the concentration Tb-NPs. The Tb and La content of the NP solutions were determined by ICP/AES (Varian 720 spectrometer equipped with a quartz Meinhard nebulizer and a cyclone spray chamber) on the mother aqueous solution of NPs previously sonicated for 10 min in an ultrasound bath and strongly agitated on a vortex prior to pipetting the sample. Mineralization of the sample was performed by pipetting 1 mL of the solution diluted in 3 mL of high purity nitric acid and heating the solution in a microwave oven at 200°C for 45 min. The La and Tb contents were determined by comparison with commercial standards. The concentration of the NPs were calculated assuming a density of the $La_{0.9}Tb_{0.1}F_3$ NPs corresponding to the averaged density of 90% of pure LaF_3 (5.936 $g.cm^{-3}$) and 10% of pure TbF_3 (7.23 $g.cm^{-3}$). The volumes of the NPs were estimated based on a spherical model with an average size corresponding to that obtained by the TEM analysis.

Synthesis and purification of ligand capped Tb-NPs. 4 mL of a 0.66 µM solution of $La_{0.9}Tb_{0.1}F_3$ NPs and 12 mL of a 0.5 mM solution of L_{11} were stirred at room temperature for 1 day at pH 7.4. The mixture was purified by size exclusion chromatography (Sephadex G75, milliQ water) and green luminescent fractions containing the capped NPs were separated and recovered.

Characterization of the ligand capped Tb-NPs. Absorption and emission spectra (Figure S4), PL decay curves (Figure S5) and photophysical properties (Table S1) of the different Tb-NP batches can be found in the Supporting Information. Batches 1 and 3: UV/vis absorption spectra were recorded on a Perkin-Elmer lambda 950 spectrometer. Steady-state PL spectra were recorded on an Edinburgh Instrument FLP920 spectrometer working with a continuous 450W Xe Lamp and a red sensitive photomultiplier in Peltier housing. All spectra were corrected for the instrumental functions. When necessary, a 399 nm cutoff filter was used to eliminate second-order artifacts. PL decays were measured on the same instrument working in the Multi Channel Scaling (MCS) mode, using a Xenon flash lamp as the excitation source. Batch 2: UV/vis absorption spectra were recorded on a Perkin-Elmer lambda 35 spectrometer. Steady-state PL spectra were recorded on a Xenius Fluorescence spectrometer (SAFAS, Monaco). PL decays were measured on Fluorescence Lifetime Platereader (Edinburgh Instruments). PL quantum yields were measured by comparison to standards,[35] using optically diluted solutions (optical density < 0.05) of rhodamine 6G in water ($\Phi = 0.76$)[36], a Tb complex prepared in the laboratory ([TbL(H_2O)]Na, $\Phi = 0.31$)[37], or a commercial Lumi4-Tb complex ($\Phi = 0.60$) in aqueous solution as references. Errors on absolute quantum yields are estimated to ±50 %. For the calculation of the extinction coefficients of the capped-NPs, the measured UV-visible absorption spectrum was deconvoluted into a linear combination of two contributions corresponding to the absorption spectrum of the capping ligands and that of the NPs. The absorption coefficient was determined using the absorption of the ligand only and the number of ligands per NP was obtained by dividing this absorption coefficient by the absorption coefficient of the ligand alone.

Cell culture. Human cervical carcinoma (HeLa) cells were purchased from American Type Culture Collection (CCL-2). Cells were grown in Dulbecco's modified eagle medium (DMEM,

Sigma-Aldrich, D6546), supplemented with 10% Fetal bovine serum (FBS, Sigma-Aldrich, F0804), 1% antibiotics (Pen Strep, Sigma-Aldrich, P4333) and 2 mM L-glutamine (Sigma-Aldrich, G7513) at 37 °C and 5% CO¬2. The cells were passaged with trypsin-EDTA 0.05%.

Cell incubation with Tb-NPs. HeLa cells were seeded at $3x10^5$ cells/dish in a CELLview petri dish with a borosilicate bottom (175 µm +/- 15 µm) and incubated at 37°C and 5% CO_2 overnight. The following day, the cells were washed with Dulbecco's Phosphate buffered saline (DPBS, D8537, Sigma-Aldrich) and incubated with a complete culture medium (10% FBS, 1% Pen Strep and 2 mM L-glutamine) supplemented with 10 mM HEPES (Sigma-Aldrich, H3375). Solution of Tb-NPs in water was sonicated for 20 minutes and added at ~ 1; 0.1 or 0.01 nM into previously prepared petri dish with cells. Cells were incubated at 37°C and 5% CO_2 for 1, 3, 6, 24 or 72h.

Co-staining with $DiOC_6(3)$ and DiD. For inner membranes labeling on HeLa cells, $DiOC_6(3)$ probe (3,3'-dihexyloxacarbocyanine iodide, D273, Molecular Probes, Eugene) was used. First, cells were suspended using trypsin in 1 ml of complete culture medium. Then, $DiOC_6(3)$ in DMF was added at the final concentration of 0.5 µM and gently mixed. Cells were incubated for 10 minutes at 37°c and 5% CO_2. In order to remove not internalized $DiOC_6(3)$ molecules, cells were washed three times using centrifugation at 1500 rpm and 37°C for 5 min. After each spin, cells were resuspended in a fresh complete culture medium. Afterwards, cells were seeded in a CELLview (Greiner, 627860) petri dish and incubated for 2h at 37°C and 5% CO_2. For the double staining experiment, cells were incubated with Tb-NPs for 4h or 24h at 0.1 nM at 37°C and 5% CO_2 in a complete culture medium supplemented with 10 mM HEPES. The same protocol was used for plasma membrane staining on HeLa cells using DID probe (1,1'-dioctadecyl-3,3,3',3'-tetramethylindodicarbocyanine, 4-chlorobenzenesulfonate salt, D7757, Molecular Probes, Eugene)

at the final concentration of 5 µM. Then, cells were incubated with Tb-NPs for 24h at 0.1 nM at 37°C and 5% CO_2 in a complete culture medium supplemented with 10 mM HEPES.

TG-PL microscopy. Cells were transferred to the live cell chamber (Oko lab) onto the miscoscope and kept at 37°C during the acquisition time. Images of NPs were acquired using a wide-field, time-gated luminescence inverted microscope (Olympus IX71) that uses a UV laser (349 nm, 100 Hz, Nd:YLF, Triton, Spectra Physics) for pulsed excitation and an intensified CCD camera (ICCD, PI-MAX3, Princeton Instruments) for gated detection. Laser power has been significantly diminished by using neutral density filters (ND Filter OD 0.5: NDUVO5B and OD 1: NDUV10B, Thorlabs). Then, corresponding pulse energy on the sample is ~1.4 µJ. The laser beam is redirected onto the sample with a 405 nm dichroic mirror (Di02-R405, Semrock Inc.). Luminescence signal was collected with a high numerical aperture (NA=1.35), immersion oil objective (Uplaspo 60xO, Olympus) and detected using 542 nm band-pass filter (FF01-542/20-25, Semrock Inc.). Acquisition settings in Winview software controlling the camera were in general fixed at delay time: 10 µs, gatewidth: 1.9 ms, gates/exposure: 400 and intensifier gain of 100 V. Carbocyanine dye DIOC6(3) was illuminated with X-Cite 120Q mercury source (EXFO Photonic Solutions Inc.) at ~10W through a 494 nm excitation band-pass filter (FF01-494/20-25, Semrock Inc.) and 495 nm dichroic mirror (FF495-Di03, Semrock Inc.). The fluorescent signal was detected using emission filter 522 nm (BP 522/12, Delta). This time, acquisition settings in Winview software were fixed to register in steady state mode with no delay time, gatewidth: 300 ms, gates/exposure: 1 and intensifier gain of 100 V. DIC images were acquired in similar conditions: with no delay time, gatewidth: 300 ms, gates/exposure: 1, accumulations: 10 and intensifier gain at 6 V. In order to remove camera dark charge from NPs intensity on TG PL images, the background acquired in the respect of the same acquisition settings (gating sequence, laser frequency) was subtracted from the raw images. Background acquisitions have been recorded by hiding incoming light with a shutter

in front of the camera. The background images have also been acquired with an open shutter on the area with no cells and subtracted from DIC images in order to improve the contrast of these last.

Cell viability assays. HeLa cells were seeded at 7 x 10^4 cells/well in 12 wells plates (Costar, multiwall plate, 12 wells, CellBind Surface, 3336, Corning) and left for overnight adhesion at 37° C and 5% CO_2. Then, cells were incubated with NPs at 0.12 nM and 1.2 nM in complete cell medium supplemented with 10 mM HEPES. Cells were rinsed three times with PBS and 200µl MTT dissolved in PBS at 3 mg/ml was added per well to the final volume of complete medium of 2 ml. Cells were incubated for 2h at 37° C and 5% CO_2. In order to solubilize the formazan crystals, 200 µl of DMSO was added per well for 30 minutes and the solution was homogenized. The same protocol was applied to the control wells, not incubated with NPs. Absorbance (optical density: OD) was measured using Spectro Star Nano (BMG Labtech) at 570 nm.

Spot detection. The presence of the NPs inside the cells was analyzed using Icy (Institut Pasteur). Cell area was determined from DIC images and respective ROIs transposed on time-gated photoluminescence images. In this way, NPs present inside the cells were analyzed using a spot detector plugin with no specific size selection. Data such as mean spot area (μm^2), spot size (pixels), spots number and Tb-NPs intensity (counts) were collected.

Z-stacking microscopy. In order to avoid high fluorescent background from culture medium HeLa cells co-stained with Tb-NPs and DiD were immersed in OptiMEM I reduced serum medium (Fisher Scientific, 11520386) supplemented with 10 mM HEPES. Fluorescent images of HeLa cells were acquired on a wide-field inverted microscope Olympus IX83 (Olympus) using X-Cite Exacte illumination source (Excelitas Technologies) and iXon Ultra 888 EMCCD camera (Andor). Tb-NPs were excited with 100W source power using 320 nm excitation filter (FF01-320/40-25, Semrock Inc.) and 355 dichroic mirror (Di01-R355, Semrock Inc.) and their emission collected

using 542 nm filter (FF01-542/20-25, Semrock Inc.). DiD was excited with 10W illumination power using 623 nm band-pass filter (FF01-623/24-25, Semrock Inc.) and 649 nm dichroic mirror (FF649-Di01, Semrock Inc.) and emission collected with 676 nm filter (FF01-676/29-25, Semrock Inc.). Sample was imaged using Uplaspo 60xO objective (Olympus). Z-stack images were obtained by a displacement of a step of 0.25 µm. Images of Tb-NPs were acquired with x750 EM gain, 30 MHz readout speed, 1.1 µs vertical shift speed and x2 pre-amplifier sensitivity. Images of plasma membrane stained with DiD were acquired with the same parameters except EM gain at x2. iXon camera and Olympus microscope were controlled by Micro-manager software in multi-dimensional acquisition window.

Tb-NP PL decay measurements in cells. Cells were incubated with Tb-NPs for 24h. Before measurement cell medium was supplemented with 10 mM HEPES. CELLview petri dish was installed in a live cell chamber under the microscope (IX71Olympus) and a highly photoluminescent cell has been chosen with the binocular. Then, a small area containing a unique cell with several luminescent vesicles was selected using a mechanical shutter of the lifetime measuring setup (Delta prototype, Horiba Jobin Yvon). The setup was trigged by the same laser used for time-gated imaging (349 nm, 80 Hz, Nd:YLF, Triton, Spectra Physics). The excitation light was reflected on the sample by a 405 nm dichroic mirror (Di02-R405, Semrock Inc.) and transmitted by immersion oil objective (Uplaspo 60xO, Olympus) on the sample. Luminescence signal was filtered through a 542 nm band pass filter (FF01-542/20-25, Semrock Inc.). and collected on a PMT detector. The corresponding decay curve was acquired in a multi channel scaling mode during 11 ms and at 2666.672 ns/channel. The curve was analyzed with FAST software (Edinburgh Photonics) using tail fitting.

Acknowledgment. The authors thank the French Agence National de la Recherche (ANR project "neutrinos") and the European Commission (Horizon2020, FET-Open project "PROSEQO") for financial support.

Supporting Information. TEM images (Figure S1) and X-ray diffraction diagram (Figure S2) of Tb-NPs from batch 2; photographs of Tb-NPs (Figure S3); absorption, excitation and emission spectra (Figure S4), PL decays (Figure S5), and photophysical properties (Table S1) of Tb-NPs; influence of pH on HeLa cells (Figure S6); Tb-NP quantitation in HeLa cells (Figure S7 and Figure S8). The Supporting Information is available free of charge on the ACS Publications website at …

REFERENCES

(1) Petryayeva, E.; Algar, W. R.; Medintz, I. L.: Quantum Dots in Bioanalysis: A Review of Applications Across Various Platforms for Fluorescence Spectroscopy and Imaging. *Applied Spectroscopy* **2013**, *67*, 215-252.
(2) Wegner, K. D.; Hildebrandt, N.: Quantum dots: bright and versatile in vitro and in vivo fluorescence imaging biosensors. *Chemical Society Reviews* **2015**, *44*, 4792-4834.
(3) Ding, H.; Cheng, L. W.; Ma, Y. Y.; Kong, J. L.; Xiong, H. M.: Luminescent carbon quantum dots and their application in cell imaging. *New Journal of Chemistry* **2013**, *37*, 2515-2520.
(4) Lim, S. Y.; Shen, W.; Gao, Z. Q.: Carbon quantum dots and their applications. *Chemical Society Reviews* **2015**, *44*, 362-381.
(5) Feng, L. H.; Zhu, C. L.; Yuan, H. X.; Liu, L. B.; Lv, F. T.; Wang, S.: Conjugated polymer nanoparticles: preparation, properties, functionalization and biological applications. *Chemical Society Reviews* **2013**, *42*, 6620-6633.
(6) Reisch, A.; Klymchenko, A. S.: Fluorescent Polymer Nanoparticles Based on Dyes: Seeking Brighter Tools for Bioimaging. *Small* **2016**, *12*, 1968-1992.
(7) Wu, C. F.; Chiu, D. T.: Highly Fluorescent Semiconducting Polymer Dots for Biology and Medicine. *Angewandte Chemie-International Edition* **2013**, *52*, 3086-3109.
(8) Haziza, S.; Mohan, N.; Loe-Mie, Y.; Lepagnol-Bestel, A. M.; Massou, S.; Adam, M. P.; Le, X. L.; Viard, J.; Plancon, C.; Daudin, R.; Koebel, P.; Dorard, E.; Rose, C.; Hsieh, F. J.; Wu, C. C.; Potier, B.; Herault, Y.; Sala, C.; Corvin, A.; Allinquant, B.; Chang, H. C.; Treussart, F.; Simonneau, M.: Fluorescent nanodiamond tracking reveals intraneuronal transport abnormalities induced by brain-disease-related genetic risk factors. *Nature Nanotechnology* **2017**, *12*, 322-328.
(9) Montalti, M.; Cantelli, A.; Battistelli, G.: Nanodiamonds and silicon quantum dots: ultrastable and biocompatible luminescent nanoprobes for long-term bioimaging. *Chemical Society Reviews* **2015**, *44*, 4853-4921.
(10) Wu, X.; Chen, G. Y.; Shen, J.; Li, Z. J.; Zhang, Y. W.; Han, G.: Upconversion Nanoparticles: A Versatile Solution to Multiscale Biological Imaging. *Bioconjugate Chemistry* **2015**, *26*, 166-175.
(11) Prodi, L.; Rampazzo, E.; Rastrelli, F.; Speghini, A.; Zaccheroni, N.: Imaging agents based on lanthanide doped nanoparticles. *Chemical Society Reviews* **2015**, *44*, 4922-4952.
(12) Dong, H.; Du, S. R.; Zheng, X. Y.; Lyu, G. M.; Sun, L. D.; Li, L. D.; Zhang, P. Z.; Zhang, C.; Yan, C. H.: Lanthanide Nanoparticles: From Design toward Bioimaging and Therapy. *Chemical Reviews* **2015**, *115*, 10725-10815.
(13) Bouzigues, C.; Gacoin, T.; Alexandrou, A.: Biological Applications of Rare-Earth Based Nanoparticles. *ACS Nano* **2011**, *5*, 8488-8505.
(14) Sy, M.; Nonat, A.; Hildebrandt, N.; Charbonniere, L. J.: Lanthanide-based luminescence biolabelling. *Chemical Communications* **2016**, *52*, 5080-5095.
(15) Dos Santos, M. C.; Hildebrandt, N.: Recent developments in lanthanide-to-quantum dot FRET using time-gated fluorescence detection and photon upconversion. *TRAC - Trends in Analytical Chemistry* **2016**, *84*, 60-71.
(16) Zwier, J.; Hildebrandt, N.: Time-gated FRET detection for multiplexed biosensing. In *Reviews in Fluorescence 2016*; Geddes, C. D., Ed.; Springer International, 2017.
(17) Delgado, D. M.; Moller, T. C.; Ster, J.; Giraldo, J.; Maurel, D.; Rovira, X.; Scholler, P.; Zwier, J. M.; Perroy, J.; Durroux, T.; Trinquet, E.; Prezeau, L.; Rondard, P.; Pin, J. P.: Pharmacological evidence for a metabotropic glutamate receptor heterodimer in neuronal cells. *Elife* **2017**, *6*.

(18) Afsari, H. S.; Dos Santos, M. C.; Linden, S.; Chen, T.; Qiu, X.; Henegouwen, P.; Jennings, T. L.; Susumu, K.; Medintz, I. L.; Hildebrandt, N.; Miller, L. W.: Time-gated FRET nanoassemblies for rapid and sensitive intra- and extracellular fluorescence imaging. *Science Advances* **2016**, *2*.
(19) Chen, Y.; Chi, Y. M.; Wen, H. M.; Lu, Z. H.: Sensitized luminescent terbium nanoparticles: Preparation and time-resolved fluorescence assay for DNA. *Anal. Chem.* **2007**, *79*, 960-965.
(20) Zhao, Q.; Liu, Y. H.; Cao, Y. F.; Lv, W.; Yu, Q.; Liu, S. J.; Liu, X. M.; Shi, M.; Huang, W.: Rational Design of Nanoparticles with Efficient Lanthanide Luminescence Sensitized by Iridium(III) Complex for Time-Gated Luminescence Bioimaging. *Advanced Optical Materials* **2015**, *3*, 233-240.
(21) Sun, W.; Yu, J. B.; Deng, R. P.; Rong, Y.; Fujimoto, B.; Wu, C. F.; Zhang, H. J.; Chiu, D. T.: Semiconducting Polymer Dots Doped with Europium Complexes Showing Ultranarrow Emission and Long Luminescence Lifetime for Time-Gated Cellular Imaging. *Angewandte Chemie-International Edition* **2013**, *52*, 11294-11297.
(22) Goetz, J.; Nonat, A.; Diallo, A.; Sy, M.; Sera, I.; Lecointre, A.; Lefevre, C.; Chan, C. F.; Wong, K. L.; Charbonniere, L. J.: Ultrabright Lanthanide Nanoparticles. *Chempluschem* **2016**, *81*, 526-534.
(23) Wang, L.; Yan, J.; Fu, P. P.; Parekh, K. A.; Yu, H. T.: Photomutagenicity of cosmetic ingredient chemicals azulene and guaiazulene. *Mutat. Res.-Fundam. Mol. Mech. Mutagen.* **2003**, *530*, 19-26.
(24) Tobi, S. E.; Gilbert, M.; Paul, N.; McMillan, T. J.: The green tea polyphenol, epigallocatechin-3-gallate, protects against the oxidative cellular and genotoxic damage of UVA radiation. *Int. J. Cancer* **2002**, *102*, 439-444.
(25) McMillan, T. J.; Leatherman, E.; Ridley, A.; Shorrocks, J.; Tobi, S. E.; Whiteside, J. R.: Cellular effects of long wavelength UV light (UVA) in mammalian cells. *J. Pharm. Pharmacol.* **2008**, *60*, 969-976.
(26) Hahn, A. T.; Jones, J. T.; Meyer, T.: Quantitative analysis of cell cycle phase durations and PC12 differentiation using fluorescent biosensors. *Cell Cycle* **2009**, *8*, 1044-1052.
(27) Oh, N.; Park, J. H.: Endocytosis and exocytosis of nanoparticles in mammalian cells. *Int. J. Nanomed.* **2014**, *9*, 51-63.
(28) de Chaumont, F.; Dallongeville, S.; Chenouard, N.; Herve, N.; Pop, S.; Provoost, T.; Meas-Yedid, V.; Pankajakshan, P.; Lecomte, T.; Le Montagner, Y.; Lagache, T.; Dufour, A.; Olivo-Marin, J. C.: Icy: an open bioimage informatics platform for extended reproducible research. *Nature Methods* **2012**, *9*, 690-696.
(29) Zhou, J.; Tan, S. H.; Nicolas, V.; Bauvy, C.; Yang, N. D.; Zhang, J. B.; Xue, Y.; Codogno, P.; Shen, H. M.: Activation of lysosomal function in the course of autophagy via mTORC1 suppression and autophagosome-lysosome fusion. *Cell Research* **2013**, *23*, 508-523.
(30) Ganley, I. G.; Carroll, K.; Bittova, L.; Pfeffer, S.: Rab9 GTPase regulates late endosome size and requires effector interaction for its stability. *Molecular Biology of the Cell* **2004**, *15*, 5420-5430.
(31) Terasaki, M.; Reese, T. S.: Characterization of endoplasmic-reticulum by colocalization of bip and dicarbocyanine dyes. *Journal of Cell Science* **1992**, *101*, 315-322.
(32) Baggaley, E.; Weinstein, J. A.; Williams, J. A. G.: Time-Resolved Emission Imaging Microscopy Using Phosphorescent Metal Complexes: Taking FLIM and PLIM to New Lengths. In *Luminescent and Photoactive Transition Metal Complexes as Biomolecular Probes and Cellular Reagents*; Lo, K. K. W., Ed.; Springer-Verlag Berlin: Berlin, 2015; Vol. 165; pp 205-256.
(33) Bui, A. T.; Grichine, A.; Duperray, A.; Lidon, P.; Riobe, F.; Andraud, C.; Maury, O.: Terbium(III) Luminescent Complexes as Millisecond-Scale Viscosity Probes for Lifetime Imaging. *J. Am. Chem. Soc.* **2017**, *139*, 7693-7696.
(34) Grichine, A.; Haefele, A.; Pascal, S.; Duperray, A.; Michel, R.; Andraud, C.; Maury, O.: Millisecond lifetime imaging with a europium complex using a commercial confocal microscope under one or two-photon excitation. *Chem. Sci.* **2014**, *5*, 3475-3485.
(35) Lakowicz, J. R.: *Principles of fluorescence spectroscopy*; 3rd ed.; Springer: New York, N.Y., 2006.
(36) Olmsted, J.: Calorimetric determinations of absolute fluorescence quantum yields. *Journal of Physical Chemistry* **1979**, *83*, 2581-2584.
(37) Weibel, N.; Charbonniere, L. J.; Guardigli, M.; Roda, A.; Ziessel, R.: Engineering of highly luminescent lanthanide tags suitable for protein labeling and time-resolved luminescence imaging. *J. Am. Chem. Soc.* **2004**, *126*, 4888-4896.